

# Charge-exchange reaction cross sections and the Gamow-Teller strength for double beta decay

K. Amos\*

*School of Physics, University of Melbourne, Victoria 3010, Australia*

Amand Faessler<sup>†</sup> and V. Rodin<sup>‡</sup>

*Institute of Theoretical Physics, University of Tuebingen, 72076 Tuebingen, Germany*

(Dated: June 18, 2018)

## Abstract

The proportionality between single charge-exchange reaction cross sections in the forward direction as found, for example from  $(p, n)$  and  $({}^3\text{He}, t)$  and from  $(n, p)$  and  $(d, {}^2\text{He})$  reactions, and the Gamow-Teller (GT) strength into the same final nuclear states has been studied and/or assumed often in the past. Using the most physically justified theory we have at our disposal and for the specific example of the  ${}^{76}\text{Ge}$ - ${}^{76}\text{Se}$  system that may undergo double beta-decay, we demonstrate that the proportionality is a relative good assumption for reactions changing a neutron into a proton, i.e.  ${}^{76}\text{Ge}(p, n){}^{76}\text{As}$ . In this channel, the main contribution to the GT strengths comes from the removal of a neutron from an occupied single-particle (SP) state and putting a proton into an unoccupied SP state having either the same state quantum numbers or those of the spin-orbit partner. In contrast to this, in the second leg of the double beta decay a single proton must be taken from an occupied SP state and a neutron placed in an unoccupied one. This second process often is Pauli forbidden in medium-heavy nuclei and only can be effected if the Fermi surface is smeared out. Such is the case for  ${}^{76}\text{Se}(n, p){}^{76}\text{As}$ . Our results suggest that one may not always assume a proportionality between the forward-angle cross sections of the charge-exchange reactions and the GT strength in any such medium-heavy nuclei. The discrepancy originates from a pronounced effect of the radial dependence of the nucleon-nucleon ( $NN$ ) interaction in connection with the Pauli principle on the cross sections in the  $(n, p)$  reaction channel. Such a radial dependence is completely absent in the GT transition operator.

## I. INTRODUCTION

In recent years, interest in the relation between charge-exchange reactions in the forward direction and the GT strength has increased due to the connection of the GT strength with the two-neutrino double beta decay [1, 2]. The latter process may help to test the nuclear wave functions required in calculations of the matrix elements for the neutrinoless double beta decay. The neu-

trinoless double beta-decay transition probability is important since it, in conjunction with measured data and assuming that the light neutrino exchange is the leading contribution, defines an absolute scale for the mass of the Majorana neutrino (for reviews see, e.g., [3, 4, 5]). The two-neutrino double beta decay matrix element  $M^{2\nu}$  is given by a sum over all intermediate  $1^+$  states of product of the GT transition matrix element from the ground state of the initial nucleus (in our example  ${}^{76}\text{Ge}$ ) to an  $1^+$  state in the intermediate nucleus ( ${}^{76}\text{As}$ ) and the GT transition matrix elements from the intermediate state to the ground state of the final nucleus ( ${}^{76}\text{Se}$ )

---

\*Electronic address: amos@physics.unimelb.edu.au

<sup>†</sup>Electronic address: amand.faessler@uni-tuebingen.de

<sup>‡</sup>Electronic address: vadim.rodin@uni-tuebingen.de

divided by the corresponding energy denominator. However, a test of the two-neutrino double beta-decay calculations using the GT strengths extracted from the measured electron capture (EC) and the single-beta decay of the intermediate nucleus is only possible if the ground state in the intermediate nucleus is a  $1^+$  state (not the case for  $^{76}\text{As}$ ), and if the two-neutrino double beta decay is dominated by the transition through this state. Our interest with the mass-76 systems in part stems from the fact that for the neutrinoless double beta-decay matrix element in past evaluations gave values ranging from 2.23 to 5 according to the chosen model of nuclear structure [6].

Complementary to the direct measurement of the GT strength by the EC capture in the first leg followed by a  $\beta^-$  transition from the lowest  $1^+$  state of the intermediate nucleus, are single-charge transfer reactions like  $(p, n)$  and  $(^3\text{He}, t)$  on the ground state of the initial nucleus and  $(n, p)$  and  $(d, ^2\text{He})$  to the ground state of the final nucleus; all connecting by the intermediate  $1^+$  states. If the forward cross section of these charge-exchange reactions are proportional to the corresponding GT strength, the two-neutrino double beta-decay probability calculations can be checked, although the information about the relative phases of different contribution can not be extracted from the experimental  $B(GT)$ . Then it is possible to test the quality of the calculations for the neutrinoless double beta decay.

The proportionality between the forward single charge-exchange cross section and the GT transition probabilities has been studied extensively in the past. Refs. [7] and [8] are particular contributions. Taddeucci et al. [7] present an interesting analytic study of the proportionality involving the single charge-exchange reaction  $(p, n)$  cross section at zero-momentum transfer which we take as quite typical of all studies of the problem. They assumed that only angular momentum transfer  $L = 0$  is important at forward scatter-

ing angles and that the eikonal approximation is valid to describe the relative motion of the incoming and emergent nucleons. Under those assumptions, they obtained an expression for the proportionality between the forward charge-exchange reaction cross section and the GT transition probability, both to  $1^+$  states. However, in that study [7] there are a number of other assumptions, many of which are questionable. First, a single particle-hole configuration is assumed for the structure of the nuclear transitions. They also assume that the reaction mechanism can be taken in either a plane or a distorted wave impulse approximation. Furthermore, the radial wave functions for the initial neutron and for the final proton in the  $(p, n)$  reaction are assumed identical and the effects of antisymmetrization between the projectile and the target nucleon is treated rather crudely. Limiting themselves to use the impulse approximation means that they use  $NN$  amplitudes in calculations and not a specific finite ranged  $NN$  interaction. They use expressions given by Franey and Love [9] which were derived from the SP84 amplitudes for free  $NN$  scattering. The nuclear medium has dramatic effects in making the effective interactions between projectile and every bound nucleon in the target quite different to the free  $NN$  case [10]. Similar concerns exist even with some of the limitations are removed, for example by using the distorted wave impulse approximation or by using phenomenology to define relative motion wave functions in a distorted wave approximation (DWA) approach. Such concerns we outline later in the text.

Ejiri [6, 11] has also made extensive study of the proportionality link. In his review [6], the proportionality of the forward charge-exchange cross section for  $(p, n)$  and  $(^3\text{He}, t)$  are shown in Figs. 10 and 15 for Fermi and GT transitions, respectively. The proportionality of the charge-exchange reaction cross section to the GT strength corresponding to a  $(n, p)$  reaction is depicted in that

review by using ( $d, {}^2\text{He}$ ) in Fig. 12, by using ( $t, {}^3\text{He}$ ) in Fig. 17 and by using ( ${}^7\text{Li}, {}^7\text{Be}$ ) in Fig. 18. Ejiri found that the proportionality with the forward scattering cross sections from single charge-exchange reactions with type  $(p, n)$  to the GT strength was good for all nuclei to mass  $A = 124$ . However, proportionality studies for the charge-exchange reaction of the type  $(n, p)$  was investigated only for masses to  $A = 12$ . Nuclei relevant for the double beta-decay proportionality of those charge-exchange reactions to the GT strengths were not considered. Such are needed of course as they are important for the two-neutrino double beta decay in the second leg where a proton changes into a neutron. Often that change cannot be effected by the GT operator  $\tau^\pm\sigma$  which can only change particle types in orbits having the same quantum numbers or into the spin-orbit partner of that level.

There have been many previous studies seeking nuclear matrix elements from experimental data with ref. [12] the most recent. Cole *et al.* [12] studied charge-exchange reactions from  ${}^{58}\text{Ni}$ . This nucleus is medium mass but it has a neutron excess of only 2. The degree of Pauli blocking to differentiate between isospin raising and lowering transitions then is small. The case should be classed with those of most light mass studies. The cases we consider on the other hand have a sizeable neutron excess and so the Pauli blocking effects in the  $(n, p)$  reactions are much more important than in the  $(p, n)$  cases.

We consider the proportionality question again but make use of the best available reaction codes to evaluate cross sections for the charge-exchange  $(p, n)$  and  $(n, p)$  reactions. We consider specifically the very popular double beta-decay transitions  ${}^{76}\text{Ge} \rightarrow {}^{76}\text{As} \rightarrow {}^{76}\text{Se}$ . The nuclear structure of the initial, the intermediate and the final states in these nuclei have been defined using the Quasiparticle Random Phase Approximation (QRPA) with realistic forces (Bonn CD potential [13]) and with matrix elements calcu-

lated by solving the Bethe-Goldstone equation [14, 15]. The results show that the forward charge-exchange cross section of the type  $(p, n)$  for the first leg of the double beta decay is nicely proportional to the GT strength but that the forward reaction cross section of type  $(n, p)$  shows rather large deviations from this proportionality. The latter is due to Pauli blocking since a proton from an occupied level must be transformed into a neutron in an empty level with the same  $(n, \ell)$  quantum numbers. Due to the radial dependence of the  $NN$  interaction, the charge-exchange reaction can proceed by transition between SP orbits that differ in  $(n, \ell)$ . Such effects violate the proportionality between the forward charge-exchange ( $(n, p)$  ( $d, {}^2\text{He}$ ), ( $t, {}^3\text{He}$ ), ( ${}^7\text{Li}, {}^7\text{Be}$ ) ...) cross sections and the GT strength.

Quality of the QRPA approach for description of the GT strengths and double beta decay has a long history [3, 4, 5, 14, 15, 16, 17, 18, 19, 20]. The nuclear wave functions calculated within the QRPA have been shown to provide good description of different properties of giant multipole resonances and low-lying collective  $2^+$  and  $3^-$  states. The gross structure of the GT strength distribution as well as the position of the GT resonance in the intermediate nuclei is correctly reproduced within the QRPA provided that the particle-particle strength of realistic nucleon-nucleon interaction is slightly renormalized by a factor  $0.8 \leq g_{pp} \leq 1.0$ , depending on the model basis size [3, 4, 5].

The nuclear shell model, which nicely describes nuclear states in the sd shell of positive parity and where it is more reliable than the QRPA, is not able to describe the states relevant for double beta decay in the pf and sdg shells. The Strassbourg-Madrid collaboration [21] can only handle a basis consisting of four single-particle levels ( $1f_{5/2}, 2p_{3/2}, 2p_{1/2}, 1g_{9/2}$ ) for the nuclei in the vicinity of  ${}^{76}\text{Ge}$ . Since the spin-orbit partners  $1f_{7/2}$  and  $1g_{7/2}$  are missing in the model space, the model-independent Ikeda

sum rule [22] is strongly violated and the GT strength calculations for  $^{76}\text{Ge}$  within the shell model are not trustful.

The QRPA model for the nuclear wave functions is considered in the next Section while that of charge-exchange reaction theory is developed in Sect. III. Then, in Sect. IV we present the results and give conclusions in Sect. V

## II. NUCLEAR WAVE FUNCTIONS

The majority of calculations of the two-neutrino and the neutrinoless double beta decay have been made using the QRPA [14, 15, 16, 17]. Although the starting points of all these studies are very similar, matrix elements calculated for the neutrinoless double beta-decay transition probabilities differ. For example, those obtained in Refs. [14, 15, 16] are quite different from the ones of Ref. [17]. This is a reason to seek tests of wave functions by deriving the two-neutrino double beta-decay probability from the GT strengths between the initial and final nucleus to a large number of  $1^+$  states in the intermediate nucleus.

Herein we use wave functions obtained from QRPA calculations [14, 15] in which the Brueckner reaction matrix elements of the Bonn CD potential [13] for the  $NN$  interaction were used. The strength of the  $NN$  matrix elements in the particle-particle channel has been slightly adjusted, by a factor  $g_{pp}$ , to reproduce the experimental two-neutrino double beta-decay probability. For  $^{76}\text{Ge}$ , this value is  $g_{pp} = 0.85$  for a 9 level basis ( $pf$  and  $sdg$  major shells). We used the unquenched values  $g_{ph} = 1$  and  $g_A = 1.25$  for the particle-hole channel renormalization factor and the axial coupling constant  $g_A$ , respectively.

Any single-particle (SP) operator of the  $\beta^-$ -type can be represented in second quan-

tization as

$$\begin{aligned}\beta_{JM}^- &= \sum_{pn, m_p m_n} \langle pm_p | b_{JM} | nm_n \rangle a_p^\dagger a_n \\ &= \hat{J}^{-1} \sum_{pn} \langle p || b_J || n \rangle C^\dagger(pn, JM). \quad (1)\end{aligned}$$

In this equation,  $\hat{J} = \sqrt{2J+1}$ ,  $C^\dagger(pn, JM) = [a_p^\dagger \otimes \tilde{a}_n]^{JM}$ , and  $b_{JM}$  can be  $\tau^-$  (Fermi),  $\sigma\tau^-$  (GT), or any other operator, including ones that have  $r$ -dependence. The time reversed creation operator is defined as  $\tilde{a}_{jm}^\dagger = (-)^{j-m} a_{j-m}^\dagger$ . Edmond's version of the Wigner-Eckart theorem has been used. The definition of the spherical harmonics includes a factor  $i^l$  in order to ensure the above expression for the time-reversal operation.

The reduced matrix element of such SP operators between the ground state of a mother nucleus and an excited state of the daughter nucleus is given by

$$\begin{aligned}\langle J^\pi || \beta_J^- || 0^+ \rangle \\ = \hat{J}^{-1} \sum_{pn} \langle p || b_J || n \rangle \varrho^{(-)}(pn, J), \quad (2)\end{aligned}$$

where the elements of the transition matrices  $\varrho^{(-)}(pn, J)$  are the reduced matrix elements,

$$\varrho^{(-)}(pn, J) = \langle J^\pi || C^\dagger(pn, J) || 0^+ \rangle. \quad (3)$$

The corresponding formulae for the  $\beta^+$ -channel are obtained by the changes

$$\begin{aligned}C^\dagger(pn, J) &\rightarrow C(pn, J) \\ \varrho^{(-)}(pn, J) &\rightarrow \varrho^{(+)}(pn, J).\end{aligned} \quad (4)$$

In the RPA, a nuclear state having angular momentum  $J$  and projection  $M$ , is created by applying the phonon operator  $Q_{JM}^\dagger$  to the vacuum state  $|0_{RPA}^+\rangle$  of the initial, even-even, nucleus, i.e.

$$|JM\rangle = Q_{JM}^\dagger |0_{RPA}^+\rangle; \quad Q_{JM} |0_{RPA}^+\rangle = 0. \quad (5)$$

Introducing the quasiparticle creation and annihilation operators,  $\alpha_{\tau m \tau}^+$  and  $\alpha_{\tau m \tau}$ , ( $\tau =$

$p, n$ ) defined by the Bogolyubov transformation,

$$\begin{pmatrix} \alpha_{\tau m \tau}^+ \\ \tilde{\alpha}_{\tau m \tau} \end{pmatrix} = \begin{pmatrix} u_{\tau} & v_{\tau} \\ -v_{\tau} & u_{\tau} \end{pmatrix} \begin{pmatrix} a_{\tau m \tau}^+ \\ \tilde{a}_{\tau m \tau} \end{pmatrix}, \quad (6)$$

the phonon operator  $Q_{JM}^\dagger$  can be written within the QRPA as

$$Q_{JM}^\dagger = \sum_{pn} \left[ X_{pn}^{(J)} A^\dagger(pn, JM) - Y_{pn}^{(J)} \tilde{A}(pn, JM) \right], \quad (7)$$

where

$$A^\dagger(pn, JM) = [\alpha_p^\dagger \otimes \alpha_n^\dagger]^{JM}, \quad (8)$$

and the forward- and backward-going free variational amplitudes  $X$  and  $Y$  satisfy the matrix equation,

$$\begin{pmatrix} \mathcal{A} & \mathcal{B} \\ \mathcal{B} & \mathcal{A} \end{pmatrix} \begin{pmatrix} X^m \\ Y^m \end{pmatrix} = \mathcal{E}_m \begin{pmatrix} 1 & 0 \\ 0 & -1 \end{pmatrix} \begin{pmatrix} X^m \\ Y^m \end{pmatrix}. \quad (9)$$

Here  $m$  identifies different roots of the QRPA equations for a given  $J^\pi$  and

$$\begin{aligned} \mathcal{A} &= \langle 0_{RPA}^+ | [A, [H, A^\dagger]] | 0_{RPA}^+ \rangle, \\ \mathcal{B} &= -\langle 0_{RPA}^+ | [A, [H, \tilde{A}]] | 0_{RPA}^+ \rangle. \end{aligned} \quad (10)$$

For a realistic residual interaction, the matrices  $\mathcal{A}$  and  $\mathcal{B}$  are

$$\begin{aligned} \mathcal{A}_{pn, p'n'}^{J^\pi} &= (E_p + E_n) \delta_{pp'} \delta_{nn'} \\ &\quad - \left[ g_{pp} G(pn, p'n'; J) \right. \\ &\quad \quad \times (u_p u_n u_{p'} u_{n'} + u_p u_n u_{p'} u_{n'}) \\ &\quad - g_{ph} F(pn, p'n'; J) \\ &\quad \quad \times (u_p v_n u_{p'} v_{n'} + v_p u_n v_{p'} u_{n'}) \left. \right], \\ \mathcal{B}_{pn, p'n'}^{J^\pi} &= \left[ g_{pp} G(pn, p'n'; J) \right. \\ &\quad \quad \times (u_p u_n v_{p'} v_{n'} + v_p v_n u_{p'} u_{n'}) \\ &\quad - g_{ph} F(pn, p'n'; J) \\ &\quad \quad \times (u_p v_n v_{p'} u_{n'} + v_p u_n u_{p'} v_{n'}) \left. \right], \end{aligned}$$

where  $G(pn, p'n', J)$  and  $F(pn, p'n', J)$  are particle-particle and particle-hole interaction matrix elements of a G-matrix, respectively.

Within the QRPA, one has

$$C^\dagger(pn, JM) = u_p v_n A^\dagger(pn, JM) + v_p u_n \tilde{A}(pn, JM), \quad (11)$$

and the transition matrix takes the form,

$$\begin{aligned} \varrho^{(-)}(pn, J) &= \hat{J}(u_p v_n X_{pn}^{(J)} + v_p u_n Y_{pn}^{(J)}), \\ \varrho^{(+)}(pn, J) &= \hat{J}(v_p u_n X_{pn}^{(J)} + u_p v_n Y_{pn}^{(J)}). \end{aligned} \quad (12)$$

Correspondingly, the  $B(GT)$  values for the GT transitions  $0^+ \rightarrow 1^+$  can be written as

$$\begin{aligned} B(GT^{(-)}) &= |\langle 1^+ | \sum_a \sigma_a \tau_a^- | 0^+ \rangle|^2 \\ &= \left| \sum_{pn} \langle p | | \sigma | | n \rangle \right. \\ &\quad \quad \times (u_p v_n X_{pn}^{(1^+)} + v_p u_n Y_{pn}^{(1^+)}) \left. \right|^2, \\ B(GT^{(+)}) &= |\langle 1^+ | \sum_a \sigma_a \tau_a^+ | 0^+ \rangle|^2 \\ &= \left| \sum_{pn} \langle n | | \sigma | | p \rangle \right. \\ &\quad \quad \times (v_p u_n X_{pn}^{(1^+)} + u_p v_n Y_{pn}^{(1^+)}) \left. \right|^2. \end{aligned} \quad (13)$$

In calculations, a harmonic oscillator with an oscillator length parameter  $b = 2.09$  fm has been used to specify the SP wave functions for  $^{76}\text{Ge}$  and  $^{76}\text{Se}$ . Those functions are positive at the origin. Using N=3 and N=4 oscillator shells in the QRPA calculations for transitions to  $1^+$  states in  $^{76}\text{As}$  gives a set of 23 two-quasiparticle excitations per Eq. (8) to be included, via Eqs. (7) and (5), into the QRPA phonon creation operator for  $1^+$  states in  $^{76}\text{As}$  [14, 15]. That set is shown in Table I. The individual components are identified by the label ID which will be used in the discussion of results. Of those two-quasiparticle states, the ones labelled with ID = 5, 6, 15, 16, 21 and 22 cannot be excited by the GT operator.

TABLE I: Two-quasiparticle configurations forming the QRPA structure of  $1^+$  states in  $^{76}\text{As}$  (relative to the ground state in  $^{76}\text{Se}$ ) and corresponding without pairing to particle-hole states.

q-p		q-h	q-p		q-h
ID	$n\ell j$	$n\ell j$	ID	$n\ell j$	$n\ell j$
1	$0f_{7/2}$	$0f_{7/2}$	13	$0g_{7/2}$	$0g_{9/2}$
2	$0f_{7/2}$	$0f_{5/2}$	14	$0g_{7/2}$	$0g_{7/2}$
3	$0f_{5/2}$	$0f_{7/2}$	15	$0g_{7/2}$	$1d_{5/2}$
4	$0f_{5/2}$	$0f_{5/2}$	16	$1d_{5/2}$	$0g_{7/2}$
5	$0f_{5/2}$	$1p_{3/2}$	17	$1d_{5/2}$	$1d_{5/2}$
6	$1p_{3/2}$	$0f_{5/2}$	18	$1d_{5/2}$	$1d_{3/2}$
7	$1p_{3/2}$	$1p_{3/2}$	19	$1d_{3/2}$	$1d_{5/2}$
8	$1p_{3/2}$	$1p_{1/2}$	20	$1d_{3/2}$	$1d_{3/2}$
9	$1p_{1/2}$	$1p_{3/2}$	21	$1d_{3/2}$	$2s_{1/2}$
10	$1p_{1/2}$	$1p_{1/2}$	22	$2s_{1/2}$	$1d_{3/2}$
11	$0g_{9/2}$	$0g_{9/2}$	23	$2s_{1/2}$	$2s_{1/2}$
12	$0g_{9/2}$	$0g_{7/2}$			

In Fig. 1, a set of one-body density matrix elements,  $\rho^{(+)}$  of Eq. (3) (OBDME hereafter), for the excitation of five particular  $1^+$  states out of the total 23 found is shown for each of the 23 components (ID). These are the states of special interest regarding the  $^{76}\text{Se}(n,p)$  zero-degree and/or zero-momentum transfer cross sections considered later; being the strongest of the 23 charge-exchange excitations considered. Of note is that the strongest OBDME  $\rho^{(+)}$  of the fourth state belongs to the two-quasiparticle state  $1p_{3/2} - 0f_{5/2}$  (ID=6). That component, readily excited in the charge-exchange reaction, cannot be excited by the GT operator. Thus, one may anticipate that the proportionality between the charge-exchange reaction cross section and the GT strength for this state may be different to those of others.

### III. REACTION THEORY

The charge-exchange reaction is described in a DWA in which one requires transition

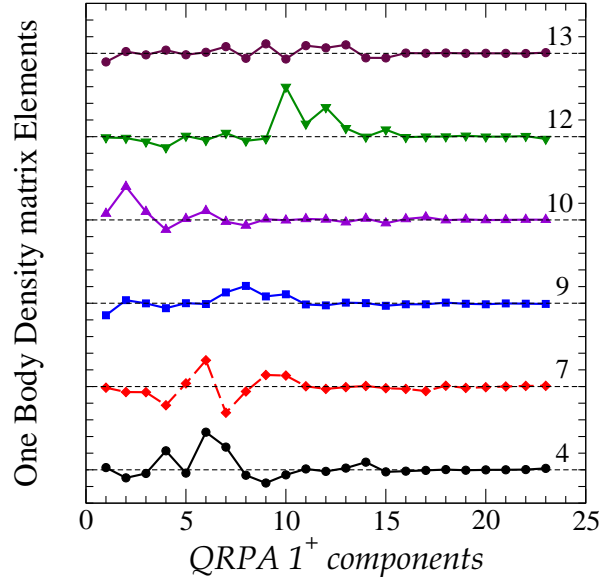


FIG. 1: (Color online) One-body density matrix elements  $\rho^{(+)}(pn, 1^+)$  of Eq. (12), in arbitrary units, for six QRPA states 4, 7, 9, 10, 12, 13 defined in Table II as functions of the two-quasiparticle components labeled according to Table I.

structure details, optical model wave functions (the distorted waves), and a transition operator by which the reaction is effected.

#### A. The optical potentials

Conventionally distorted wave functions are the relative motion wave functions ascertained from an optical potential with which good fits to elastic scattering data (cross section and spin observables) have been obtained. In many studies those potentials have been assumed to be local in form and usually of Woods-Saxon type with parameters adjusted to find a good fit to elastic scattering data. But the associated relative motion wave functions are not guaranteed to be proper. Only the asymptotic (large radius) properties are tested by such data fitting since one only requires the scattering phase shifts which are then used in Legendre poly-

nomial sums that define the cross sections etc. There are other concerns about phenomenological model potentials to be noted. The most serious concern is the violation of the Pauli principle. A local potential assuming smooth parameter variations with energy will support bound and resonance states of the compound system, and the projectile can be captured in any. But the set includes states that are densely occupied in the actual target. Further the resonances are then all single particle in nature and it is known that all nuclei support compound and quasi-compound ones as well. For low energy scattering one needs a better reaction theory, such as the multi-channel algebraic scattering theory (MCAS) to do better. Studies with that MCAS approach [23, 24] have revealed that when coupled-channel effects are important then the effects of violation of the Pauli principle with potential-like models are most severe, and worse can lead to erroneous Physics. This is one reason why we consider energies at which specific coupled-channel effects, such as of virtual excitation of the giant resonances, are minor if not negligible. Coupling to states in the continuum [25] has been investigated, but, without taking into account the effects of the Pauli principle in the optical potentials, that result lacks some credibility. No doubt such may have a marked role in reactions such as break-up and inelastic scattering into the continuum, but we do not consider such coupling to the continuum as the transitions of interest are to specific isolated states of given spin-parity. For such, we have found no case as yet for which the basic  $g$ -folding method (described next), when defined with good spectroscopy, requires additional reaction processes to give reasonable results.

A more physical approach is to form optical potentials by folding an  $NN$  interaction with the target ground state structure. In that way one can also ensure that the Pauli principle is not violated. However, once the target structure has been set, then one has

to choose the  $NN$  interaction. For some time now it has been known that the interaction differs from the free  $NN$  one. Medium effects lead to the effective  $NN$  interaction being energy- and density-dependent as well as complex. The current best practice, at least for energies below 3-3 resonance excitation, is to use an effective interaction built from the  $NN$   $g$ -matrices that are solutions of the Bethe-Brueckner-Goldstone (BBG) equations [10]. Using those  $g$ -matrices, both on- and off-shell values and for 32  $NN$  angular momentum channels, lead to an effective  $NN$  interaction in coordinate space that is a mixture of central, two-nucleon spin-orbit, and two-nucleon tensor components. Details of that mapping are given elsewhere [10].

Of great importance is that on using such an effective  $NN$  interaction in forming optical potentials, and when account is taken of the Pauli principle, those optical potentials are strongly non-local and partial wave dependent. Non-locality arises from the allowance for knock-out (exchange) amplitudes in the so-called  $g$ -folding procedure [10]. Doing so requires more than just the densities of the nuclear ground state. One requires the ground state OBDME

$$\rho_{gs} = \langle 0_{gs}^+ | [a_j^\dagger \otimes \tilde{a}_j]^{(J=0)} | 0_{gs}^+ \rangle. \quad (14)$$

Assuredly, the relative motion wave functions will differ from those found using phenomenological (local) potentials even if the potentials are phase equivalent. The Perey effect is one ramification. Exchange effects are also most important in evaluations of non-elastic scattering and that will be discussed later.

In coordinate space, the  $g$ -folding optical potential can be written

$$\begin{aligned} U(\mathbf{r}, \mathbf{r}'; E) &= \delta(\mathbf{r} - \mathbf{r}') \int \rho(\mathbf{s}) g^D(\mathbf{r}, \mathbf{s}; E) d\mathbf{s} \\ &+ \sum_i n_i \varphi_i^*(\mathbf{r}) g^{Ex}(\mathbf{r}, \mathbf{r}'; E) \varphi_i(\mathbf{r}'); \\ \rho(\mathbf{s}) &= \sum_i n_i \varphi_i^*(\mathbf{s}) \varphi_i(\mathbf{s}). \end{aligned} \quad (15)$$

Here  $\rho(\mathbf{s})$  is the nucleon density for nucleons with the occupancies  $n_i$ . To evaluate these potentials requires specification of three quantities. They are the single nucleon bound state wave functions  $\varphi_i(\mathbf{r})$ , the orbit occupancies  $n_i$ , which more properly are the nuclear OBDME of Eq. (14), and the  $NN$   $g$ -matrices  $g^{D/Ex}(\mathbf{r}, \mathbf{s}; E)$ .

### B. The effective interaction between projectile and bound nucleons

The  $g$ -matrices in the equation above, are appropriate combinations of  $NN$  interactions in the nuclear medium for diverse  $NN$  angular momentum channels. For those  $NN$  interactions, much success has been had using an effective  $NN$  interaction, now commonly designated as the Melbourne force [10], and which has the form  $g_{01}^{ST} \equiv g_{eff}^{ST}(\mathbf{r}, E; k_f(R))$  where  $\mathbf{r} = \mathbf{r}_0 - \mathbf{r}_1$  and  $R = \frac{1}{2}|\mathbf{r}_0 + \mathbf{r}_1|$ . It is based on the  $g$ -matrix of the Bonn  $B$  potential [26]. In the prescription, the Fermi momenta relate to the local density in the nucleus at distance  $R$  from the center when  $\mathbf{r}_i$  are the coordinates of the colliding projectile and bound nucleons.  $\{ST\}$  are the spin and isospin quantum numbers of the  $NN$  system.

For use in the DWBA98 program [27], these effective  $NN$   $g$ -matrices are, specifically,

$$\begin{aligned} g_{eff}^{ST} &= g_{eff}^{ST}(\mathbf{r}, E; k_f) \\ &= \sum_{i=1}^3 \left[ \sum_{j=1}^4 S_j^{(i)}(E; k_f) \frac{e^{-\mu_j^{(i)} r}}{r} \right]_{[S,T]} \Theta_i \\ &= \sum_{i=1}^3 g_{eff}^{(i)ST}(r, E; k_f) \Theta_i, \end{aligned} \quad (16)$$

where  $\Theta_i$  are the characteristic operators for central forces ( $i = 1$ ),  $\{1, (\sigma \cdot \sigma), (\tau \cdot \tau), (\sigma \cdot \sigma \tau \cdot \tau)\}$ , for the tensor force ( $i = 2$ ),  $\{\mathbf{S}_{12}\}$ , and for the two-body spin-orbit force ( $i = 3$ ),  $\{\mathbf{L} \cdot \mathbf{S}\}$ . The  $S_j^{(i)}(E; k_f)$  are complex, energy- and density-dependent strengths. The properties of the  $g$ -matrices are such that, not

only can the ranges of the Yukawa form factors be taken as independent of energy and density [10], but also four suffice with this approach for energies to just below the 3-3 resonance threshold.

The strengths (and ranges) in these effective  $NN$  interactions were found by mapping their double Bessel transforms to the  $NN$   $g$ -matrices in infinite nuclear matter (solutions of the BBG equations). With  $\alpha: \{LL'JST\}$ , this mapping is

$$g_{\text{eff};LL'}^{JST}(q', q; E) = \sum_i \langle \Theta_i \rangle \mathcal{I}_i, \quad (17)$$

where the radial integrals expand to

$$\begin{aligned} \mathcal{I}_i &= \int_0^\infty r^{2+\lambda} j_L(q'r) g_{\text{eff}}^{(i)ST}(r, E; k_f) j_{L'}(qr) dr \\ &= \sum_j S_j^{(i)}(\omega) \\ &\quad \times \int_0^\infty r^{2+\lambda} j_L(q'r) \frac{e^{-\mu_j^{(i)} r}}{r} j_{L'}(qr) dr \\ &= \sum_j S_j^{(i)}(\omega) \tau^\alpha(q', q; \mu_j^{(i)}). \end{aligned} \quad (18)$$

Therein  $\lambda = 2$  for the tensor force. In application, a singular valued decomposition has been used to effect this mapping.

### C. The DWA for non-elastic reaction analyses

In the DWA, amplitudes for a non-elastic scattering of nucleons from nuclei, through a scattering angle of  $\theta$ , and between the states  $|J_i, M_i\rangle$  and  $|J_f, M_f\rangle$ , are

$$\begin{aligned} T_{DWA} &= T_{J_f J_i}^{M_f M_i \nu \nu}(\theta) \\ &= \left\langle \chi_{\nu'}^{(-)}(\mathbf{k}_0 0) \left| \left\langle \Psi_{J_f M_f}(1 \cdots A) \right. \right. \right. \\ &\quad \times A \sum_{ST} g_{eff}^{ST}(\mathbf{r}_{0,1}, E; k_f) P_S P_T \\ &\quad \left. \left. \left. \times \mathcal{A}_{01} \left\{ \left| \chi_{\nu'}^{(+)}(\mathbf{k}_i 0) \right\rangle \left| \Psi_{J_i M_i}(1 \cdots A) \right\rangle \right\} \right. \right. \end{aligned} \quad (19)$$



where  $\nu, \nu'$  are the spin quantum number of the nucleon in the continuum,  $\chi^{(\pm)}$  are the distorted waves, and  $g_{eff}^{ST}(\mathbf{r}_{0,1}, E; k_f P_S P_T)$  is the spin-isospin Melbourne force. The operator  $\mathcal{A}_{01}$  effects the antisymmetrization of the two-nucleon product states.

Then, by using cofactor expansions,  $|\Psi_{JM}\rangle = A^{-1/2} \sum_{j,m} |\varphi_{jm}(1)\rangle a_{jm} |\Psi_{JM}\rangle$ , the matrix elements become

$$\begin{aligned} T_{J_f J_i}^{M_f M_i \nu \nu'} &= \sum_{j_1, j_2 i, S, T} \langle \Psi_{J_f M_f} | a_{j_2 m_2}^\dagger a_{j_1 m_1} | \Psi_{J_i M_i} \rangle \\ &\times \left\langle \chi_{\nu'}^{(-)}(\mathbf{k}_0 0) \left| \left\langle \varphi_{j_2 m_2}(1) \right| g_{eff}^{ST}(\mathbf{r}_{0,1}, E; k_f) \right. \right. \\ &\left. \left. \times P_S P_T \mathcal{A}_{01} \left\{ \left| \chi_{\nu}^{(+)}(\mathbf{k}_i 0) \right\rangle \left| \varphi_{j_1 m_1}(1) \right\rangle \right\} \right. \right. \end{aligned} \quad (20)$$

The density matrix elements in the amplitudes reduce as

$$\begin{aligned} &\left\langle \Psi_{J_f M_f} \left| a_{j_2 m_2}^\dagger a_{j_1 m_1} \right| \Psi_{J_i M_i} \right\rangle \\ &= \sum_{I(N)} (-1)^{(j_1 - m_1)} \langle j_1, j_2, m_1, -m_2 | I, N \rangle \\ &\times \left\langle \Psi_{J_f M_f} \left| \left[ a_{j_2}^\dagger \otimes a_{j_1} \right]^{IN} \right| \Psi_{J_i M_i} \right\rangle \\ &= \sum_{I(N)} (-1)^{(j_1 - m_1)} \langle j_1, j_2, m_1, -m_2 | I, N \rangle \\ &\times \langle J_i, I, M_i, N | J_f, M_f \rangle \frac{1}{\sqrt{2J_f + 1}} S_{j_1 j_2 I}, \end{aligned} \quad (21)$$

where  $S_{j_1 j_2 I}$  are the transition OBDME. The DWA amplitudes are then

$$\begin{aligned} T_{J_f J_i}^{M_f M_i \nu \nu'} &= \sum_{\xi} \frac{(-)^{(j_1 - m_1)}}{\sqrt{2J_f + 1}} S_{j_1, j_2, I} \\ &\times \langle j_1, j_2, m_1, -m_2 | I, N \rangle \langle J_i, I, M_i, N | J_f, M_f \rangle \\ &\times \left\langle \chi_{\nu'}^{(-)}(\mathbf{k}_0 0) \left| \left\langle \varphi_{j_2 m_2}(1) \right| \mathbf{g}_{eff}^{ST}(\mathbf{r}_{0,1}, E; k_f) \right. \right. \\ &\left. \left. \times P_S P_T \mathcal{A}_{01} \left\{ \left| \chi_{\nu}^{(+)}(\mathbf{k}_i 0) \right\rangle \left| \varphi_{j_1 m_1}(1) \right\rangle \right\} \right. \right. \end{aligned} \quad (22)$$

In this,  $\{\xi\} = j_1, j_2, m_1, m_2, I(N), S, T$  with  $j_2$  being the particle and  $j_1$  the hole in a particle-hole specification of the transition.

Thus, in our DWA evaluations of the charge-exchange scattering of interest, namely  $^{76}\text{Ge}(p, n)$  and  $^{76}\text{Se}(n, p)$  to  $1^+$  states given by a QRPA model, we have used

1. SP wave functions: harmonic oscillators with oscillator length of 2.09 fm. Those are used to specify both the optical potentials and the reaction amplitudes.
2. Optical potentials (to give the distorted waves) are formed with the Melbourne effective  $NN$  interaction at the relevant incident particle energies. The occupancies of the single particle level are automatically given in the QRPA due to pairing and configuration mixing and are contained in the OBDME in Eq. (12).
3. The same effective interactions are used in evaluations of the charge-exchange cross sections.
4. The  $\rho^{(\pm)}$  of Eq. (12) are taken as the  $S_{j_1, j_2, I=1}$  depending upon which reaction,  $(p, n)$  or  $(n, p)$ , is described.

## IV. RESULTS

We have stressed the importance of using an appropriate optical model to define the distorted wave functions in DWA evaluations of the charge-exchange scattering. We contend that potentials formed using the  $g$ -folding procedure are such for incident nucleon energies in the range  $\sim 40$  to  $\sim 300$  MeV and for nuclei for which, at the minimum, sensible models of their ground state structures can be specified.

For the mass-76 nuclei we consider specifically, very few nucleon scattering results have been reported. We have found data for the scattering of 22.3 MeV protons from both  $^{76}\text{Ge}$  and  $^{76}\text{Se}$  [28] and for 64.5 MeV proton scattering from  $^{76}\text{Se}$  [29] (see fig. 2). For nucleon scattering off of these targets, 22.3

MeV may be too low an energy to have confidence that the reaction processes not included in the  $g$ -folding method, e.g. coupled-channel effects, multi-step processes, and the like, may have importance. For energies 40 MeV and higher, such extra processes have not been needed to find good replication of elastic scattering data with  $g$ -folding model evaluations [10, 30, 31, 32, 33, 34, 35], when good structure, and appropriate effective  $NN$  interactions are used, and a proper treatment of the Pauli principle is made.

In this study, we have chosen four incident energies at which the transition to the lowest  $1^+$  state in  $^{76}\text{As}$  is considered. Those energies are 45, 65, 120, and 200 MeV. Subsequently, for our investigation of transitions to all 23  $1^+$  state excitations, we have used just the two largest energies of 120 and 200 MeV. Proton elastic scattering data have been taken for all four energies and from many targets. With most cases,  $g$ -folding model analyses [10] gave good reproductions of the observations, especially whenever good models for the structure of the target were available. Besides results given in the review [10], in more recent studies the  $g$ -folding method has been used to assess the neutron excess distributions in nuclei [36, 37, 38, 39], to compare with non-relativistic and relativistic phenomenological Schrödinger equation solutions [30, 31], and to ascertain neutron halo or neutron skin characteristics in light mass radioactive nuclei [32, 33].

It is a mantra of  $g$ -folding studies that no adjustments to details specified are considered *post facto*. Consequently,  $g$ -folding predictions invariably do not yield the quality of fit to a data set that may be obtained by appropriate adjustment of parameters in current, phenomenological, optical potentials [40]. Nonetheless, the  $g$ -folding approach does give cross sections that compare well with observations; well enough that, in some cases, results [32, 33, 36, 38, 39] revealed whether a nucleus had a neutron skin or halo.

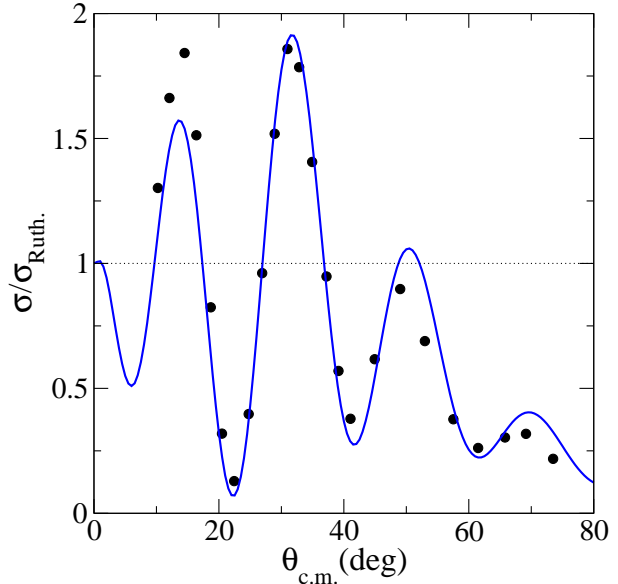


FIG. 2: Ratio to Rutherford cross sections for 64.5 MeV protons scattering from  $^{76}\text{Se}$ . The solid line represents the calculation result of this work.

An analysis of cross sections from the elastic scattering of 65 MeV protons from  $^{76}\text{Se}$  is illustrative of the quality of the  $g$ -folding potential results. That data [29], in ratio to Rutherford form, are compared in Fig. 2 with the (single calculation) result from our  $g$ -folding optical model potential of the system. With the exception of the forward peak, our prediction compares favorably with the result of the phenomenological optical potential calculation of Ogino *et al* [29]. The agreement with data from our non-phenomenological approach suffices to give confidence that the non-local, complex, optical potential formed fully microscopically is a credible, physically justified, one. It is important to note that there is no addition of any phenomenological elements as used in what may be termed semi-microscopic methods [25, 41].

### A. $(p, n)$ reactions to $1^+$ states in $^{76}\text{As}$

Differential cross sections evaluated at zero-degree scattering and the total reaction cross sections from  $^{76}\text{Ge}(p, n)$  and  $^{76}\text{Se}(n, p)$  leading to the first  $1^+$  state in  $^{76}\text{As}$  are displayed in Fig. 3. The results found at energies of 45, 65, 120, and 200 MeV, are connected by solid lines ( $0^\circ$  cross sections) and by dashed lines (reaction cross sections). The results of  $^{76}\text{Ge}(p, n)$  to the first excited  $1^+$  state in  $^{76}\text{As}$  are larger than those of  $^{76}\text{Se}(n, p)$  to the same first excited  $1^+$  state. Over these energies, those ratios range from 25 to 65. It is intriguing that both the zero-degree differential cross sections, which increase with energy, and the reaction cross sections, which decrease accordingly, have such similar ratios.

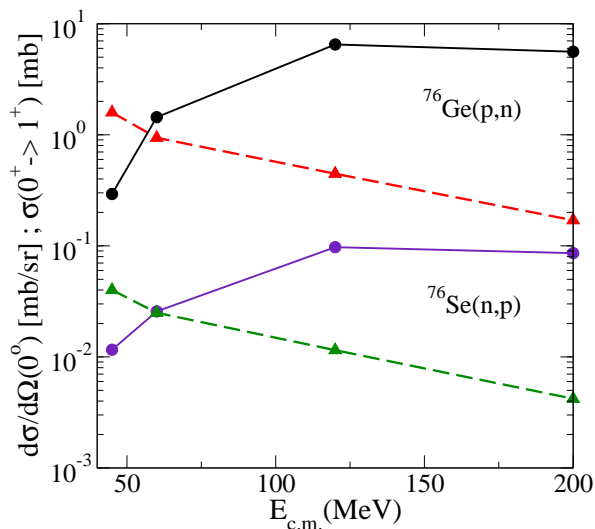


FIG. 3: (Color online) Zero-degree differential cross sections (filled circles) and total reaction cross sections (filled triangles) from  $^{76}\text{Ge}(p, n)$  and  $^{76}\text{Se}(n, p)$  leading to  $^{76}\text{As}(1_1^+, 0.947 \text{ MeV})$ .

The scale factors are not simply a zero-degree phenomenon. This is emphasized by the differential cross-section results for the four energies displayed in Fig. 4 for a small range of momentum transfer  $q_{cm}$  from 0. The results

in the top of this figure for the four energies as indicated, are those from the charge-exchange  $(p, n)$  reaction. The other (smaller in magnitude) results are differential cross sections for the  $(n, p)$  reaction. The scale factors are an effect of the Pauli principle. In  $^{76}\text{Ge}_{44}$ , the proton Fermi surface lies between the  $1p_{3/2}$  and the  $0f_{5/2}$  levels while the neutron Fermi surface lies within the  $0g_{9/2}$  single-particle state. For the  $(p, n)$  charge-exchange reaction, one must move a neutron into a proton level. In these nuclei the GT transition operator  $\tau^-\sigma$  can make a nucleon into a single particle level with the same quantum numbers or to the spin-orbit partner. This is possible for transitions  $0f_{5/2} \rightarrow 0f_{5/2}$ ,  $1p_{1/2} \rightarrow 1p_{1/2}$  and  $0g_{9/2} \rightarrow 0g_{9/2}$ . But for the inverse reaction,  $(n, p)$  on  $^{76}\text{Se}_{42}$ , all the possible single-particle GT transitions are strongly Pauli hindered, if not Pauli blocked. The latter cases allow GT transitions since the GT operator can only move a proton into a corresponding neutron level of the same  $(nlj)$  orbit or the spin-orbit partner because of the smearing of the Fermi surface which is mainly induced by pairing correlations. For the charge-exchange reaction  $(n, p)$  on the other hand, the finite range character of the transition operator and the knock-out process associated with antisymmetrization allow non-GT type transitions to contribute.

The energy variation in magnitudes of these results for each reaction separately reflects the energy dependence of the contributing terms to the charge exchange process in the effective  $NN$  interaction. Tensorial components, which do not contribute strongly to the charge exchange processes we consider herein, nonetheless vary in importance in the overall prescription of the medium modified force [10] with energy and with angular momentum transfer [34, 35]. Above 100 MeV these cross sections are essentially of the same magnitude and so we consider the two energies, 120 and 200 MeV, in the subsequent

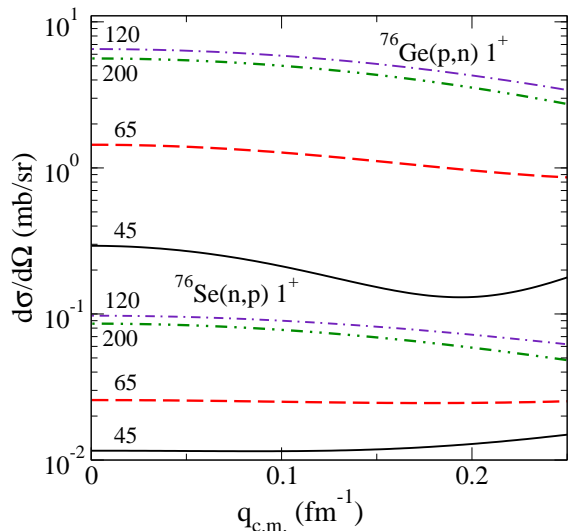


FIG. 4: (Color online) Differential cross sections from the two charge-exchange reactions leading to the first  $1^+$  state in  $^{76}\text{As}$  for bombarding energies of 45 (solid curves), 65 (dashed curves), 120 (dot-dashed curves) and 200 (double dot-dashed curves) MeV.

discussions. We note that, for all four energies, and for those of 120 and 200 in particular, cross sections smoothly decrease away from the zero-momentum transfer values over the small momentum transfer values considered. Furthermore, while the momentum transfer values for zero-degree scattering at these two energies are small but non-zero, evaluations of cross sections setting energies to give a zero-momentum transfer gave values less than a percent different from those of the actual zero-degree calculations.

The foregoing dealt only with the excitation of the first  $1^+$  state in  $^{76}\text{As}$ . We now consider the zero-degree cross sections for all 23 possible  $1^+$  states defined by the QRPA and their ratios to the corresponding GT strengths. Shown in table II those cross-section values for the  $^{76}\text{Ge}(p,n)$  and  $^{76}\text{Se}(n,p)$  reactions to each of the 23 excited  $1^+$  states are listed in columns 2 and 4. The ratios of those with the corresponding GT strengths are listed in columns 3 and 5.

TABLE II: differential cross sections at zero degrees scattering for the charge-exchange reactions  $^{76}\text{Ge}(p,n)$  and  $^{76}\text{Se}(n,p)$  exciting  $^{76}\text{As}(1^+, m)$ . The projectile energy in all cases was 200 MeV.  $\nabla$  are the ratios of each of those cross sections with the associated, dimensionless, GT strength. The calculated excitation energy  $E_x$  of the  $1^+$  states is measured from the ground state of  $^{76}\text{Ge}$ .

$m$	$E_x$ , MeV	$^{76}\text{Ge}(p,n)(0^\circ)$	$\nabla$	$^{76}\text{Se}(n,p)(0^\circ)$	$\nabla$
1	1.16	5.61	3.73	0.09	3.15
2	2.10	1.74	5.55	$1 \times 10^{-3}$	25.48
3	2.41	1.01	5.27	0.03	10.96
4	2.87	2.35	6.19	0.22	6.93
5	3.14	1.07	3.80	$3 \times 10^{-4}$	571.43
6	3.41	3.04	4.95	$3 \times 10^{-3}$	40.12
7	3.95	12.28	4.16	0.26	3.71
8	4.86	2.31	3.56	0.08	3.54
9	5.16	15.01	3.96	0.38	3.10
10	6.39	0.34	5.45	0.18	6.27
11	8.40	18.43	3.47	0.04	3.40
12	9.90	4.77	4.09	0.31	3.83
13	11.25	3.98	4.21	0.24	4.29
14	11.44	9.40	4.01	0.01	4.77
15	12.31	10.05	4.05	0.05	3.63
16	12.60	51.52	4.02	0.01	3.91
17	12.82	1.49	3.93	$3 \times 10^{-4}$	8.93
18	13.47	0.08	3.94	$2 \times 10^{-3}$	4.25
19	13.63	0.14	4.14	0.01	4.16
20	14.37	0.27	3.98	0.02	3.92
21	15.01	$5 \times 10^{-3}$	4.10	$2 \times 10^{-5}$	3.20
22	16.71	0.02	4.87	$7 \times 10^{-4}$	6.13
23	17.36	0.10	4.21	0.02	4.58

State 16 corresponds to excitation of the GT resonance that is reflected by the large  $(p,n)$  cross section at zero-degree scattering being 51 mb/sr. The corresponding GT strength has a dimensionless value of 12.8. The states 7, 9, 11, 15 and 16 have differential  $(p,n)$  cross sections at zero-degree scattering larger

than 10 mb/sr. The ratio to the GT strength for these five states are 4.16, 3.96, 3.47, 4.05 and 4.02. The ratio for these five leading states therefore lies between 3.47 and 4.16; and so there is about 20% variation relative to the mean value. The six largest values for the  $^{76}\text{Se}(n,p)$  cross section at zero-degree scattering are obtained for the states identified as 4, 7, 9, 10, 12 and 13 in the sequence. The ratios of these cross sections to their corresponding GT strengths vary between 3.1 and 6.9. Thus for these six largest  $(n,p)$  transitions, there is a variation in the ratio of the zero-degree charge-exchange cross section to the GT strength of about 80%. This is large in comparison to the variation in the ratios involving the strongest  $(p,n)$  reaction cross sections.

In fig. 5 the zero-degree cross sections for  $^{76}\text{Ge}(p,n)^{76}\text{As}(1^+,m)$ ;  $m = 1, \dots, 23$  are shown by the filled circles connected by dashed lines. The filled squares connected by solid lines are the dimensionless GT strengths of the operator of eq. (13),  $B(GT^{(-)}, ^{76}\text{Ge} \rightarrow ^{76}\text{As})$ , for transition to each state of the QRPA given in sequence in table II. The charge-exchange cross section values, connected by the dashed lines, resulted from DWA calculations made using the full  $NN$  interaction (Melbourne force) as the transition operator. The open circles are results obtained when only the central part of that transition operator was used. Clearly, for zero-degree scattering, the two-body spin-orbit and tensor contributions do not effect the cross sections appreciably. The proton incident energy for all  $(p,n)$  reactions is 200MeV.

Clearly the zero-degree cross sections for all  $(p,n)$  transitions track similarly to the GT strengths of the same states. For the  $(p,n)$ , and presumably also for the corresponding reactions ( $^3\text{He}, t$ ), the proportionality between those charge-exchange reaction cross sections in the forward direction and the GT strengths

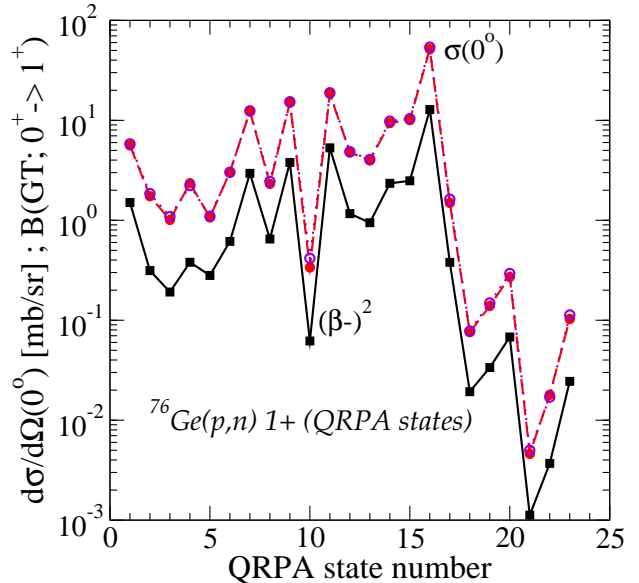


FIG. 5: (color online) differential cross sections at zero-degree scattering from DWA calculations of  $^{76}\text{Ge}(p,n)^{76}\text{As}(1^+,m)$ . Results found with and without non-central components in the transition operator are depicted by the filled and open circles respectively. The filled squares are the values of  $B(GT^{(-)})$  for  $^{76}\text{Ge} \rightarrow ^{76}\text{As}(1^+,m)$  for each  $1^+$  state.

is fulfilled quite well. As noted above, that means a proportionality within about 20% for the five strongest transitions.

The situation is different for the  $(n,p)$  reactions, and presumably also for the corresponding reactions ( $t, ^3\text{He}$ ) and ( $^7\text{Li}, ^7\text{Be}$ ). That is evident both from inspection of the results in table II and in fig. 6. For these transitions, most components are Pauli forbidden so far as the GT operator is concerned. Finite values occur only due to a smearing of the Fermi surfaces. But the  $(n,p)$  reactions, while hindered similarly, also can proceed by excitation of other components in the wave functions.

From fig. 6 it is evident that the  $(n,p)$  cross sections variation over the 23 QRPA possi-

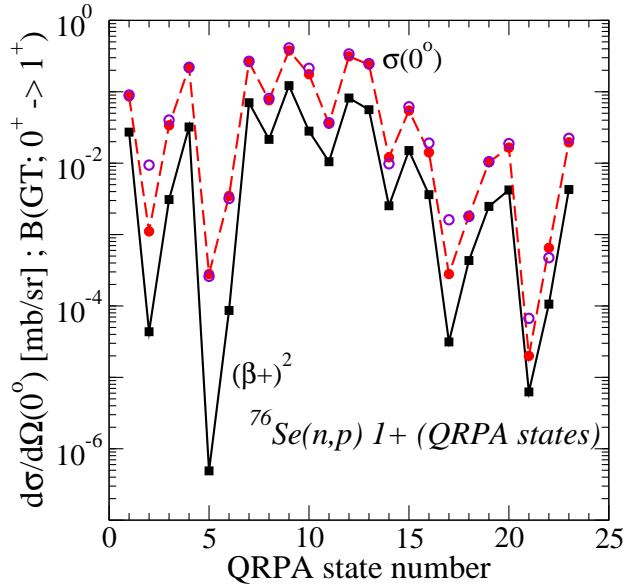


FIG. 6: (color online) differential cross sections at zero-degree scattering for  $^{76}\text{Se}(n,p)$  to the 23  $1^+$  states in  $^{76}\text{As}$  (filled circles connected by dashed lines). the DWBA results found by restricting the transition operator to just the central terms are depicted by the open circles. The associated GT strengths are shown by the filled squares connected by solid lines.

ble states still tracks the values of the associated GT strengths. However, note that both cross sections and GT strengths are much smaller than their counterparts in fig. 5, and the omission of non-central force elements in DWA calculations makes some greater variation than seen with the  $(p,n)$  results. Consequently, the proportionality ‘constant’ of the ratio of forward direction,  $(n,p)$  charge-exchange cross sections to the GT strengths for the six strongest transition is very large.

As the specifics of the Melbourne force change with incident energy, and particularly those of the non-central components, we have made DWA calculations at other energies. At 120MeV, the zero-degree cross section values and their ratios with the associated GT strengths are listed in table III. As with the 200MeV results, the proportionality be-

tween the charge-exchange cross sections calculated at zero-degree scattering and the GT strength is fulfilled to within about 20% for the reaction  $^{76}\text{Ge}(p,n)$ . However, the variation is much larger for the ratios with the cross sections for  $^{76}\text{Se}(n,p)$ . In fact the variation of the latter ratios is near 90% when one considers only the strongest  $(n,p)$  transitions.

TABLE III: the zero-degree charge-exchange cross sections and ratios ( $\nabla$ ) of them to the associated GT strength for the  $^{76}\text{Ge}(p,n)$   $^{76}\text{As}$  and  $^{76}\text{Se}(n,p)$   $^{76}\text{As}$  reactions to  $^{76}\text{As}(1^+, m)$ . In this case, the incident energy was 120MeV.

$m$	$^{76}\text{Ge}(p,n)(0^\circ)$	$\nabla$	$^{76}\text{Se}(n,p)(0^\circ)$	$\nabla$
1	6.51	4.33	0.10	3.58
2	2.40	7.64	$9 \times 10^{-3}$	210.10
3	1.47	7.67	0.05	17.26
4	2.98	7.85	0.28	8.80
5	1.32	4.70	$6 \times 10^{-4}$	1146.9
6	3.73	6.07	$2 \times 10^{-3}$	25.56
7	14.85	5.03	0.31	4.35
8	2.77	4.26	0.09	4.13
9	17.47	4.61	0.46	3.73
10	0.46	7.45	0.24	8.68
11	21.52	4.06	0.04	3.91
12	5.65	4.84	0.37	4.56
13	4.81	5.08	0.24	4.19
14	11.07	4.73	0.02	8.06
15	11.83	4.76	0.07	4.50
16	61.63	4.81	0.02	6.29
17	1.84	4.86	$2 \times 10^{-3}$	49.43
18	0.09	4.51	$2 \times 10^{-3}$	5.12
19	0.17	5.06	0.01	4.68
20	0.33	4.87	0.02	4.91
21	$6 \times 10^{-3}$	4.90	$7 \times 10^{-5}$	10.88
22	0.02	5.68	$9 \times 10^{-4}$	8.10
23	0.11	4.54	0.02	4.65

In fig. 7, the zero-degree cross sections from our DWA evaluations of all  $^{76}\text{Se}(n,p)$  reac-



tions to the QRPA  $1^+$  states in  $^{76}\text{As}$  are shown for an incident neutron energy of 120MeV. As before, those results are depicted by the filled and open circles (connected by the dashed lines to guide the eye), with the filled circle presenting the results when the complete Melbourne force is used and the open circles giving the results when only the central force components are considered. The associated GT strengths are depicted by the filled squares connected by the solid lines. As with the results for 200MeV, the  $(n, p)$  cross section values vary across the 23 QRPA cases very similarly to the GT strength values. But the devil is in the differences again and the ratio of them is far removed from being constant over the set.

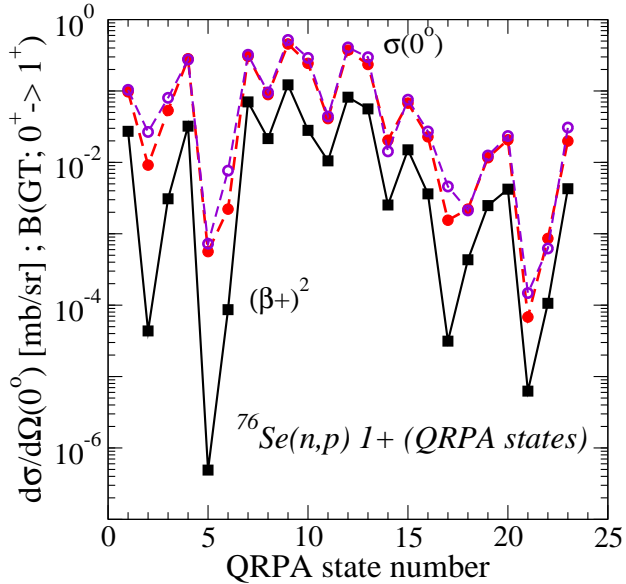


FIG. 7: (color online) zero-degree differential cross sections from DWA calculations of 120MeV  $^{76}\text{Se}(n, p)$  to  $1^+$  excited states in  $^{76}\text{As}$  and the associated GT strengths. Details are given in the text.

Finally, in figure 8 the ratios of our calculated zero-degree charge-exchange cross sections and GT strengths for the transition

$^{76}\text{Ge} \rightarrow ^{76}\text{As}$  (filled circles connected by a solid lines) to the 23 QRPA states in  $^{76}\text{As}$  and for the incident proton energy of 200MeV, are shown. The ratios for  $^{76}\text{Se}(n, p) ^{76}\text{As}$  cross sections are displayed by the open diamonds connected by dashed lines (200MeV) and by the filled triangles connected by dot-dashed lines (120MeV). On this scale the relative smoothness of the ratios for all 23 QRPA cases of  $^{76}\text{Ge} \rightarrow ^{76}\text{As}$  is apparent. The variation though is  $\sim 20\%$ . But the extreme variation over the set for the  $^{76}\text{Se}(n, p) ^{76}\text{As}$  ratios makes it impossible to consider such as forming a proportionality constant. Even restricting consideration to the five strongest  $(n, p)$  transitions yields a variation of  $\sim 90\%$ .

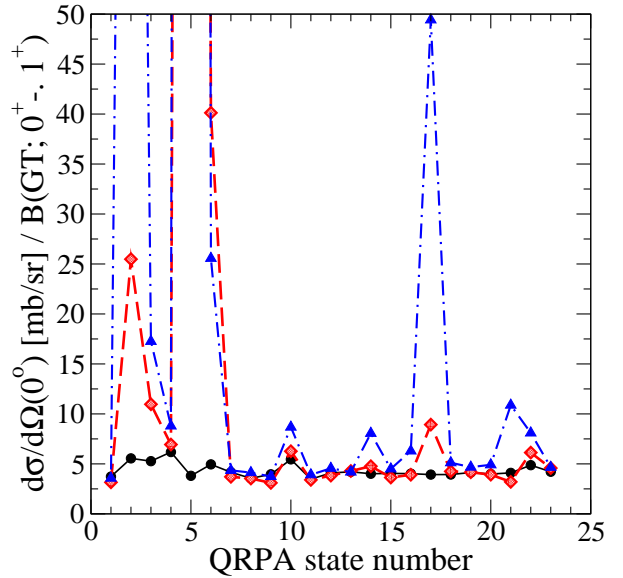


FIG. 8: (Color online) Ratios of cross sections from  $^{76}\text{Ge}(p, n) ^{76}\text{As}$  evaluated at zero degrees with the GT strengths (filled circles) for an incident energy of 200 MeV and for  $^{76}\text{Se}(n, p) ^{76}\text{As}$  as displayed for 200 MeV (open diamonds) and for 120 MeV (filled triangles).

## V. CONCLUSIONS

In conclusion, from our analysis of excitations with the QRPA model structure for the three mass-76 nuclei, the proportionality between forward differential cross sections and GT strengths is fulfilled to within about 20% for the  $^{76}\text{Ge}(p, n)$  GT transitions. But this is not the case with forward differential charge-exchange  $(n, p)$  reactions unlike the cases in light mass nuclei. In light nuclei, where protons and neutrons fill the same or nearly the same single-particle levels, the proportionality of forward charge-exchange reaction cross sections and the GT strengths seems valid for both  $(n, p)$  and  $(p, n)$  processes. For them the proton and neutron Fermi surfaces are similar. But that is not so for medium heavy nuclei such as the mass-76 set we considered herein. With them the proton and neutron Fermi surfaces are quite different, and the effects of Pauli-blocking (hindering for smeared surfaces) allows the proportionality to be good (within 20%) for  $(p, n)$  processes but not for the  $(n, p)$  transitions. This arises because the charge-exchange  $(n, p)$  transitions are sensitive to radial overlaps of single particle wave functions whereas the GT values

are not, and for the  $(n, p)$  processes those in which a nucleon stays within a given orbit but changes type are not as dominant as with the  $(p, n)$  ones.

We anticipate that such will be the case for systems that have sizeable neutron excess. It will be interesting not only to apply the approach we have taken in cases whenever relevant data are available with which additional tests of the quality of the nuclear structure model can be made but also in any case when application of theories for charge-exchange processes initiated by composite projectiles, as comparably physically justified, can be made.

### Acknowledgments

We are most grateful to Prof. Herbert Mütter for providing us with solutions of the Bethe-Goldstone equation starting with the Bonn-CD  $NN$  force. The work of V. R. has been supported by the Deutsche Forschungsgemeinschaft (by grant FA67/28-2 and within the Transregio Project TR27 “Neutrinos and Beyond”). A. F. and V. R. thank also the EU ILIAS project under the contract RII3-CT-2004-506222 for support.

- 
- [1] S. Rakers et al., Phys. Rev. C **65**, 044323 (2002).
  - [2] S. Rakers et al., Phys. Rev. C **71**, 054313 (2005).
  - [3] A. Faessler and J. Simkovic, J. Phys. **G24**, 2139 (1998).
  - [4] S. R. Elliot and P. Vogel, Ann. Rev. Nucl. Part. Sci. **52**, 115 (2002).
  - [5] R. D. McKeown and P. Vogel, Phys. Rep. **394**, 315 (2004).
  - [6] H. Ejiri, Phys. Rep. **338**, 265 (2000).
  - [7] T. N. Taddeucci et al., Nucl. Phys. **A469**, 125 (1987).
  - [8] S. Rakers et al., Phys. Rev. C **70**, 054302 (2004).
  - [9] M. A. Franey and W. G. Love, Phys. Rev. C **31**, 488 (1985).
  - [10] K. Amos, P. J. Dortmans, H. V. von Geramb, S. Karataglidis, and J. Raynal, Adv. in Nucl. Phys. **25**, 275 (2000).
  - [11] H. Ejiri, Nucl. Phys. **A687**, 350c (2001).
  - [12] A. L. Cole et al., Phys. Rev. C **74**, 034333 (2006).
  - [13] R. Machleidt, F. Sammarruca, and Y. Song, Phys. Rev. C **53**, R1483 (1996).
  - [14] V. Rodin, A. Faessler, F. Simkovic, and P. Vogel, Phys. Rev. C **69**, 044302 (2003).
  - [15] V. Rodin, A. Faessler, F. Simkovic, and P. Vogel, Nucl. Phys. **A766**, 107 (2006).
  - [16] K. Muto, Phys. Lett. **B391**, 343 (1997).
  - [17] O. Civitarese and J. Suhonen, Nucl. Phys. **A729**, 867 (2003).



- [18] T. Tomoda and A. Faessler, Phys. Lett. **B199**, 475 (1987).
- [19] P. Vogel and M. R. Zirnbauer, Phys. Rev. Lett. **57**, 3148 (1986); J. Engel P. Vogel and M. R. Zirnbauer, Phys. Rev. C **37**, 731 (1988).
- [20] K. Muto, E. Bender and H. V. Klapdor, Z. Phys. A **334**, 177 (1989).
- [21] E. Caurier, G. Martinez-Pinedo, F. Nowacki, A. Poves and A. P. Zuker, Rev. Mod. Phys. **77**, 427 (2005).
- [22] K. Ikeda, Prog. Theor. Phys. **31**, 434 (1964).
- [23] L. Canton, G. Pisent, J. P. Svenne, D. van der Knijff, K. Amos, and S. Karataglidis, Phys. Rev. Lett. **94**, 122503 (2005).
- [24] K. Amos, S. Karataglidis, D. van der Knijff, L. Canton, G. Pisent, and J. P. Svenne, Phys. Rev. C **72**, 064603 (2005).
- [25] J. Al-Khalili and F. Nunes, J. Phys. **G 29**, R89 (2003).
- [26] R. Machleidt, K. Holinde, and C. Elster, Phys. Rep. **149**, 1 (1987).
- [27] J. Raynal, *computer program dwba98, nea 1209/05* (1998).
- [28] W. H. L. Moonent, P. J. van Hall, S. S. Klein, G. J. Nijghll, C. W. A. M. van Overveldl, R. M. A. L. Petit, and . J. Poppema, J. Phys. **G 19**, 635 (1993).
- [29] K. Ogino, Phys. Rev. C **33**, 71 (1986).
- [30] P. K. Deb, K. Amos, S. Karataglidis, M. Chadwick, and D. Madland, Phys. Rev. Lett. **86**, 3248 (2001).
- [31] P. K. Deb, B. Clark, S. Hama, K. Amos, S. Karataglidis, and E. D. Cooper, Phys. Rev. C **72**, 014608 (2005).
- [32] A. Lagoyannis et al., Phys. Letts. **B 518**, 27 (2001).
- [33] S. V. Stepantsov et al., Phys. Letts. **B 542**, 35 (2002).
- [34] K. Amos, S. Karataglidis, and Y. J. Kim, Nucl. Phys. **A 762**, 230 (2005).
- [35] Y. J. Kim, K. Amos, and S. Karataglidis, Nucl. Phys. **A 779**, 82 (2006).
- [36] S. Karataglidis, B. A. Brown, K. Amos, and P. K. Deb, Phys. Rev. C **85**, 044306 (2002).
- [37] J. Klug et al., Phys. Rev. C **67**, 031601 (2003).
- [38] K. Amos, S. Karataglidis, and J. Dobaczewski, Phys. Rev. C **70**, 024607 (2004).
- [39] K. Amos, B. A. Brown, S. Karataglidis, and W. R. Richter, Phys. Rev. Lett. **96**, 032503 (2006).
- [40] A. J. Koning and J. P. Delaroche, Nucl. Phys. **A 713**, 231 (2003).
- [41] C. Joouanne et al., Phys. Rev. C **72**, 014308 (2005).